Nuclear stopping and energy loss in Au+Au collisions at $\sqrt{s_{NN}}$=62.4 GeV.

I. Arsene, T. M. Larsen, S. Lindahl, G. Løvhøiden, B. H. Samset, and T. S. Tveter
University of Oslo, Department of Physics, Oslo,Norway

I. G. Bearden, H. Bøggild, C. H. Christensen, P. Christiansen, H. H. Dalsgaard, J. J. Gaardhøje, C. E. Jørgensen, C. Nygaard, B. S. Nielsen, D. Ouerdane, C. Ristea, and P. Staszel
Niels Bohr Institute, Blegdamsvej 17, University of Copenhagen, Copenhagen 2100, Denmark

D. Beavis, C. Chasman, R. Debbe, H. Ito, J. H. Lee, and F. Videbæk
Brookhaven National Laboratory, Upton, NY 11973-5000, U.S.

S. Bekele, E. B. Johnson, D. Pal, and S. J. Sanders
University of Kansas, Lawerence, Kansas 66049

C. Besliu, A. Jipa, and O. Ristea
University of Bucharest, Romania

B. Budick
New York University, New York 10003

K. Hagel, M. Murray, J. Natowitz, and R. Wada
Texas A&M University, College Station, Texas, 17843

R. Karabowicz, N. Katrynska, Z. Majka, and R. Planeta
Smoluchkowski Inst. of Physics, Jagiellonian University, Krakow, Poland

F. Rami
Institut Pluridisciplinaire Hubert Curien and Université Louis Pasteur, Strasbourg, France

D. Röhrich, H. Yang, and Z. Yin
University of Bergen, Department of Physics and Technology, Bergen, Norway

I. S. Zgura
Institute for Space Science, Bucharest, Romania
(Dated: Version: BRAHMS Nuclear Stopping II, January 30, 2007)

Transverse momentum spectra of protons and antiprotons in the rapidity range $0 < y < 3.1$ from 0-5% central Au+Au collisions at $\sqrt{s_{NN}} = 62.4$ GeV are presented. From the spectra, measured using the BRAHMS experiment at RHIC, the rapidity densities dN/dy of protons, anti-protons and net-protons $(N(p) - N(\bar{p}))$ have been obtained. The net-proton yield is roughly constant, $dN/dy \sim 12$, for $y < 1$ but rises to $dN/dy \sim 30$ at $y > 2$. Together with data from experiments at other energies we may estimate the rapidity shift, energy loss and particle production that is to be expected at the Large Hadron Collider for Pb+Pb collisions at $\sqrt{s_{NN}} = 5500$ GeV. We predict that the LHC rapidity shift is not much larger than the one found at RHIC, $2.1 < \delta y_{LHC} < 3.4$.
PACS numbers: 25.75 Dw.

In collisions between gold nuclei at the top energy ($\sqrt{s_{NN}} = 200$ GeV) of the Relativistic Heavy Ion Collider, RHIC, a state of matter characterized by partonic (quark and gluon) degrees of freedom and with properties similar to that of a fluid is believed to have been observed ([1], [2], [3], [4], [5]). The partons are produced copiously during the initial stages of the collisions and subsequently hadronize resulting in about 7000 ([6]) particles that emerge from the collision zone and stream towards the detectors. Of these, approximately two thirds, are charged particles and can be detected using conventional techniques. The energy required for producing these particles is taken from the kinetic energy of the baryons in the colliding nuclei, who consequently experience a loss in rapidity.

The measurement of the rapidity loss of the neutrons and protons in the colliding nuclei not only determines the energy available for particle production, but also yields information on the deceleration (stopping) of the

DRAFT

ions due to their mutual interaction, primarily due to the strong interaction. The stopping may be determined by measuring the rapidity distribution of the net-protons (or, ideally, the number of net-baryons if neutral particles can be detected) after the collision. The term net-protons denotes the difference between the total number of protons, consisting of the number of protons in the colliding nuclei and the number of produced protons, and the number of antiprotons, which are all produced.

In this Letter, we present the first measurements of the rapidity shift of Au ions at $\sqrt{s_{NN}} = 62.4$ GeV. The experimental arrangement of the BRAHMS detector makes it possible to measure the distribution of net-protons over a rapidity interval ranging from $y = 0$ to $y = 3.1$. This rapidity range is wide enough to include the rapidity at which most of the protons are found after the collision, in contrast to the situation at the RHIC top energy, where the beam rapidity is higher ($y = 5.4$), but where the measurement cannot resolve this maximum baryon density peak. This situation allows to determine the rapidity shift with small errors. Together with similar information from experiments at lower energies e.g. at the AGS ($\sqrt{s_{NN}} = 10.6$ GeV) and SPS ($\sqrt{s_{NN}} = 17$ GeV) accelerators and at the RHIC top energy ($\sqrt{s_{NN}} = 200$ GeV) ([7], [8], [9]) we conclude that the rapidity loss of ultrarelativistic heavy ions exhibits a near saturating behavior as a function of beam rapidity. We exploit this observation to predict the rapidity and energy loss for heavy ions at the Large Hadron Collider (LHC), which is expected to become operational at CERN next year and which will collide lead nuclei at $\sqrt{s_{NN}} = 5500$ GeV.

We use the average rapidity loss to quantify nuclear stopping. It is defined as [10]:

$$\delta y = y_{beam} - \frac{2}{N_{part}} \int_0^{y_{beam}} y \frac{dN_{B-\bar{B}(y)}}{dy} dy \tag{1}$$

Here N_{part} is the number of participant nucleons in the collision, y_{beam} is the beam rapidity and $\frac{dN_{B-\bar{B}}}{(}y)dy$ is the net-baryon rapidity density, derived from the rapidity density of the net-protons. Related to the rapidity loss, is the energy loss, defined as:

$$\delta E = E_{beam} - \frac{2}{N_{part}} \int_0^{y_{beam}} m_T \cosh y \frac{dN_{B-\bar{B}(y)}}{dy} dy \tag{2}$$

Here, E_{beam} is the beam energy and $m_T = \sqrt{m^2 + p_T^2}$ is the transverse mass.

The BRAHMS detector operating at RHIC was used for the studies presented here. It consists of two magnetic spectrometers: the *Mid Rapidity Spectrometer* (MRS) covering polar angles (measured with respect to the beam direction) $30° < \theta < 90°$ and the *Forward Spectrometer* (FS) covering $2.3° < \theta < 15°$.Together they provide acceptance for protons in the range $-0.1 < y < 3.5$. Each spectrometer enables the tracking of charged hadrons using two Time Projection Chambers (TPC) in the MRS and two TPCs and three Drift Chambers (DC) in the FS. Collision centrality is determined using a silicon and plastic tile multiplicity array located around the intersection point. Throughout the analysis presented here, the centrality class $0 - 5\%$ was selected. The vertex determination is done using two arrays of Cherenkov counters positioned on either side of the nominal collision point. They permit determination of the interaction vertex with an accuracy better than 1.5 cm [11]. A vertex cut of $\pm 15(20)$cm is applied to tracks in MRS (FS).

Particle identification (PID) is done in the MRS using the time of flight (TOF) technique. It enables PID for protons in the momentum range 0.4 GeV/c $< p <$ 3 GeV/c. The protons used in the analysis are selected by making a $\pm 2\sigma_{m^2}$ wide cut in the m^2 vs p distributions of the particles. Kaons and protons can no longer be separated when their m^2 distributions overlap within $\pm 2\sigma_{m^2}$ of their mean m^2.

In the FS two PID detectors are used: A TOF system similar to the one in MRS and a Ring Imaging CHerenkov (RICH) detector. In the RICH protons with $p > 15$ will emit rings while lower momentum protons will emit 'rings' with radius zero. PID is done in two momentum regions: 3 GeV/c $< p <$ 7.5 GeV/c and 12 GeV/c $< p <$ 20 GeV/c, corresponding to the lower left and right spectra in Figure 1, respectively. For 3 GeV/c $< p <$ 7.5 GeV/c we require a hit in the TOF wall within $\pm 2\sigma_{m^2}$ *and* a signal in the RICH with ring radius zero. In the range 12 GeV/c $< p <$ 20 GeV/c the RICH is used exclusively for PID. For 12 GeV/c $< p <$ 16 GeV/c the protons are selected as particles with ring radius zero and for 16 GeV/c $< p <$ 20 GeV/c the selection is done by converting the rings into a m^2 and making a $\pm 2\sigma_{m^2}$ cut. For 12 GeV/c $< p <$ 16 GeV/c a correction for kaons and pions that fail to produce rings is applied. The RICH inefficiency for kaons and pions to produce rings is 3%.

Following the PID and vertex cuts the differential yields, $\frac{1}{2\pi p_T} \frac{d^2N}{dy dp_T}$ were corrected for geometrical acceptance and efficiency. The geometrical acceptance correction is based on a simulation to find the distribution of tracks that make it through the detectors. This is then compared to the number of tracks generated to calculate the correction. The efficiency of the TOF walls was found to be 93-98%. The efficiency of the tracking detectors

DRAFT

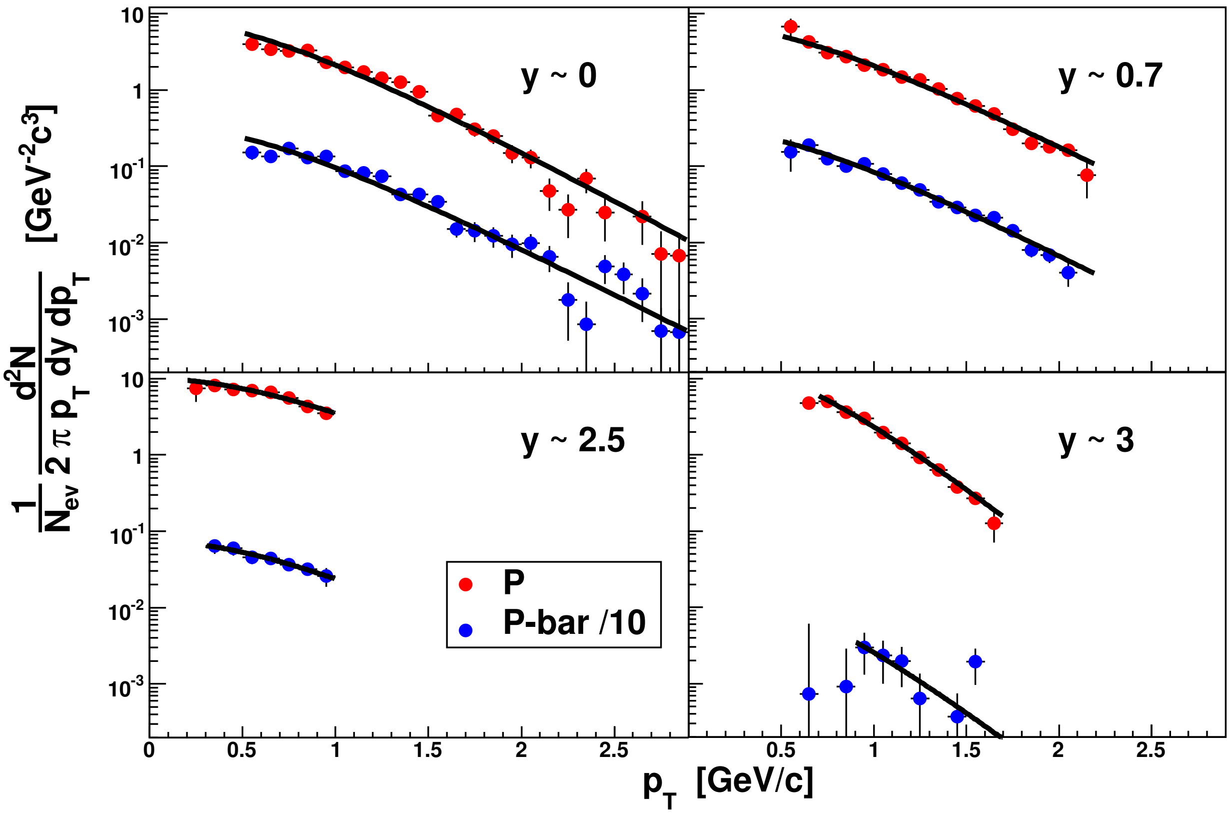

FIG. 1: Spectra of identified protons and antiprotons for $y \sim 0$, $y \sim 0.7$, $y \sim 2.5$ and $y \sim 3$ respectively. Included in the figure are the fit functions used to determine the yield. Note that the same fit ranges are used for protons and antiprotons. Vertical bars show statistical errors.

depend on their position in the spectrometers. In the MRS the total tracking efficiency was found to be $\approx 90\%$ and in the FS the total tracking efficiency was found to be $\approx 80\%$. The data was also corrected for absorption, multiple scattering and weak decays, estimated through simulations using HIJING [17] and GEANT [16]. The total corrections for these effects were less than 20% at the lowest p_T and less than 5% at the highest p_T in all settings.

Figure 1 shows the invariant spectra of protons and antiprotons for $y \sim 0$, $y \sim 0.7$, $y \sim 2.5$ and $y \sim 3$ as a function of transverse momentum, p_T. The integrated yields have been obtained by fitting the measured spectra with functions $f(m_T) \propto \frac{1}{T(T+m)} e^{\frac{-m_T - m}{T}}$ and integrating the fit functions in the range $0 < p_T < \infty$. From these we can obtain the rapidity densities, $\frac{dN}{dy}$.

The top panel of Figure 2 shows the $\frac{dN}{dy}$ of protons and antiprotons. The lower panel shows the $\frac{dN}{dy}$ of the net-protons, defined here as the difference in $\frac{dN}{dy}$ of protons and antiprotons. The systematic error associated with this procedure is determined by varying the fit function, the fit range, the bin width, choice of fit function and rapidity selection.

In order to evaluate the rapidity loss (cf. Eq. 1 for the $\sqrt{s_{NN}} = 62.4$ GeV data presented here, the net-proton rapidity density shown in Figure 2 must be fitted with a reasonable function. Inspired by [9] we use a double gaussian in longitudinal momentum, p_z:

$$\frac{dN}{dy} \propto (\exp\left[\frac{-(p_z-\mu)^2}{2\sigma^2}\right] + \exp\left[\frac{-(p_z+\mu)^2}{2\sigma^2}\right]) \tag{3}$$

An important constraint arises, since the total number of baryons is conserved. Since only protons are measured a conversion between the number of net-protons and the number of net-baryons is necessary. Using the same approach as in [9] we convert the number of net-protons, N_p, to net-baryons, N_b, using $N_b = 2.05 \cdot N_p$.

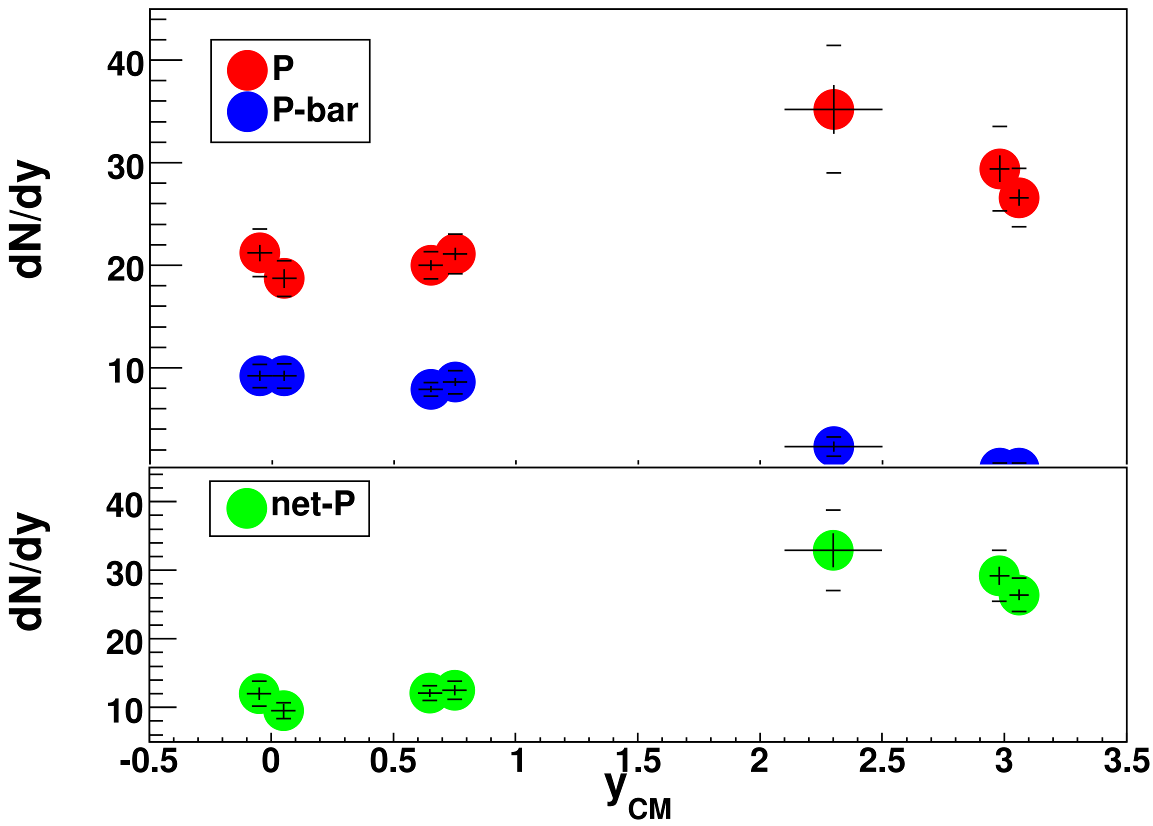

FIG. 2: Top panel: rapidity density of protons and antiprotons. Lower panel: rapidty densities of net proton. The vertical bars indicate statistical errors and the horizontal bars show the total error including the estimated systematic errors.

With this conversion the rapidity loss and energy loss at $\sqrt{s_{NN}} = 62.4$GeV is found to be

$$\delta y = 2.16 \pm 0.05, \quad \delta E = 25 \pm 1\text{GeV}$$

Thus, $\approx 80\%$ of the initial beam energy is available for particle production after the collision. The distribution in longitudinal momentum is well reproduced by Eq. 3 with parameters $\mu_{p_z} = 6.3 \pm 0.2$ GeV/c, $\sigma_{p_z} = 2.9 \pm 0.1$ GeV/c.

The rapidity losses at AGS ([7], [14] and [15]), SPS [8] and RHIC $\sqrt{s_{NN}} = 200$ GeV [9] together with the present result are presented in Figure 3. The figure shows that rapidity shifts increases rapidly with beam energy from AGS to SPS but only increases slowly from SPS energy to RHIC energies.

The set of rapidity losses have been fitted to the function:

$$f(y_{CM}) = A + B(1 - \exp(y_{CM})) \tag{4}$$

shown in Figure 3 as the solid curve. Also shown in Figure 3 as the dashed line is a linear fit to SPS through RHIC data. Taking these functions as a maximum and minimum value of the rapidity loss for $y > 5.4$, the shaded band represents the expected range of the rapidity loss. Thus, the rapidity loss at LHC must be expected to lie between $2.1 < \delta y < 3.4$. Figure 3 also includes the fit from [10] (hashed line) and it can be seen that this linear scaling breaks down already at $y_{CM} \approx 4$, in particular for RHIC 62 GeV.

At SPS energies [8] the conversion between baryons and protons is done as: $N_b = (2.07 \pm 0.05) \cdot N_p + (1.6 \pm 0.1) \cdot N_\Lambda$, where N_Λ is the number of net-lambdas. Assuming N_Λ to be constant, using $N_\Lambda = 9.3$ at midrapidity from [12] and $N_p = 26.9$ from [8] one obtains $N_b = 2.6 \cdot N_p$. From the shape of the distribution of protons from [8] this must be a maximum value, so in the following we assume $N_b = 2.5 \cdot N_p$ for SPS and AGS. At RHIC energies ($\sqrt{s_{NN}} = 62.4$ GeV and $\sqrt{s_{NN}} = 200$ GeV) where the majority of particles is produced pairwise we use $N_b = 2.0 \cdot N_p$. The number of participants for SPS is quoted in [13] to be $N_{part} = 362 \pm 12$. For AGS we assume the same number of participants as for RHIC $\sqrt{s_{NN}} = 62.4$ GeV setup, ie. $N_{part} = 337 \pm 6$

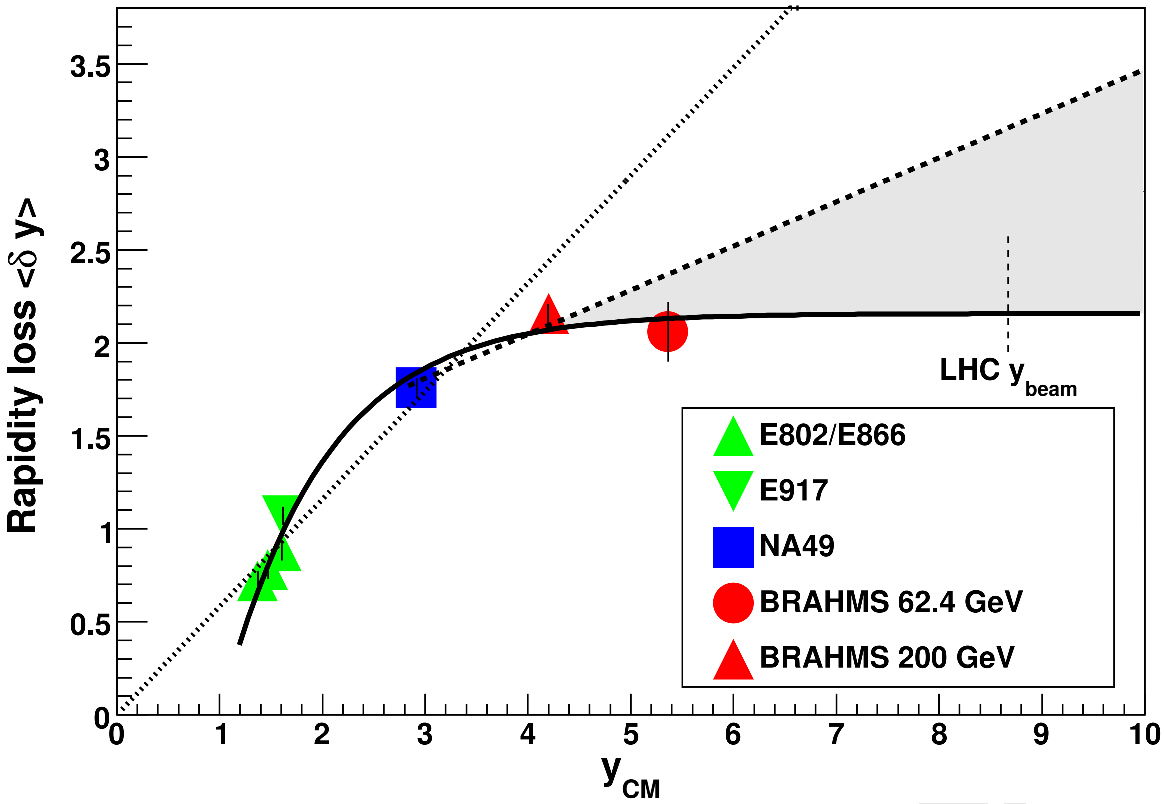

FIG. 3: Rapidity shifts from AGS, SPS and RHIC as a function of rapidity. The full drawn line is a fit using Eq. 4 in text. The dashed curve is a straight line fit. Also included is the line from [10] (hashed line)

The four top panels of Figure 4 show the net-proton $\frac{dN}{dy}$ from AGS, SPS, RHIC 62 GeV and RHIC 200 GeV. The distributions have been obtained by fitting the data plotted as a function of longitudinal momentum to Eq. 3. The integrals of the fits are constrained by the number of participants scaled with the proton-to-baryon conversion factor discussed above. The average rapidity losses obtained by this method are shown in Figure 4. They are consistent with the values found in [7], [8] and [9].

The bottom panel in Figure 4 shows the predicted net-proton distribution for Pb+Pb collisions at the LHC at $\sqrt{s_{NN}} = 5500$ GeV. It has been obtained by a linear extrapolation of the μ_{p_z} σ_{p_z} values resulting from fitting Eq. 3 to the data from AGS, SPS, RHIC 62 GeV and RHIC 200 GeV. Here N_{part} for central Pb+Pb collisions at LHC is taken to be 380. The conversion factor from protons to baryons is assumed to be the same as for RHIC, i.e. $N_b = 2 \cdot N_p$. With this distribution the expected rapidity shift and energy loss for Pb+Pb collisions at LHC is

$$\delta y = 2.8 \pm 0.1 \quad \text{and} \quad \delta E = 2323 \pm 61 \text{ GeV} \, ,$$

respectively. This indicates that about 80 % of the total kinetic energy is available for particle production. This is about the same ratio as for RHIC energies. We note that the used extrapolation of the double gaussian distribution of the number of net-protons as a function of longitudinal momentum gives a predicted rapidity loss which is in good agreement with the phenomenological extrapolations of the measured rapidity shifts indicated by the coloured area in Figure 3.

From the predicted energy loss the charged particle multiplicity expected at LHC can in principle be calculated if the charged particle mix (mainly pions, kaons, protons and light hyperons), the average transverse momentum of these particles and their rapidity distribution, is known. Assuming that all charged particles have $m_t = 800$ MeV and that the distribution of charged particles as a function of rapidity is of triangular shape betweeen $y = -8.6$ and $+8.6$ we obtain using the relation $E = m_T \cdot cosh(y)$, a charged particle multiplicity peaking at $y = 0$ with the value $dN/dy \approx 3000$. Assuming that the distribution of charged particles is flat between

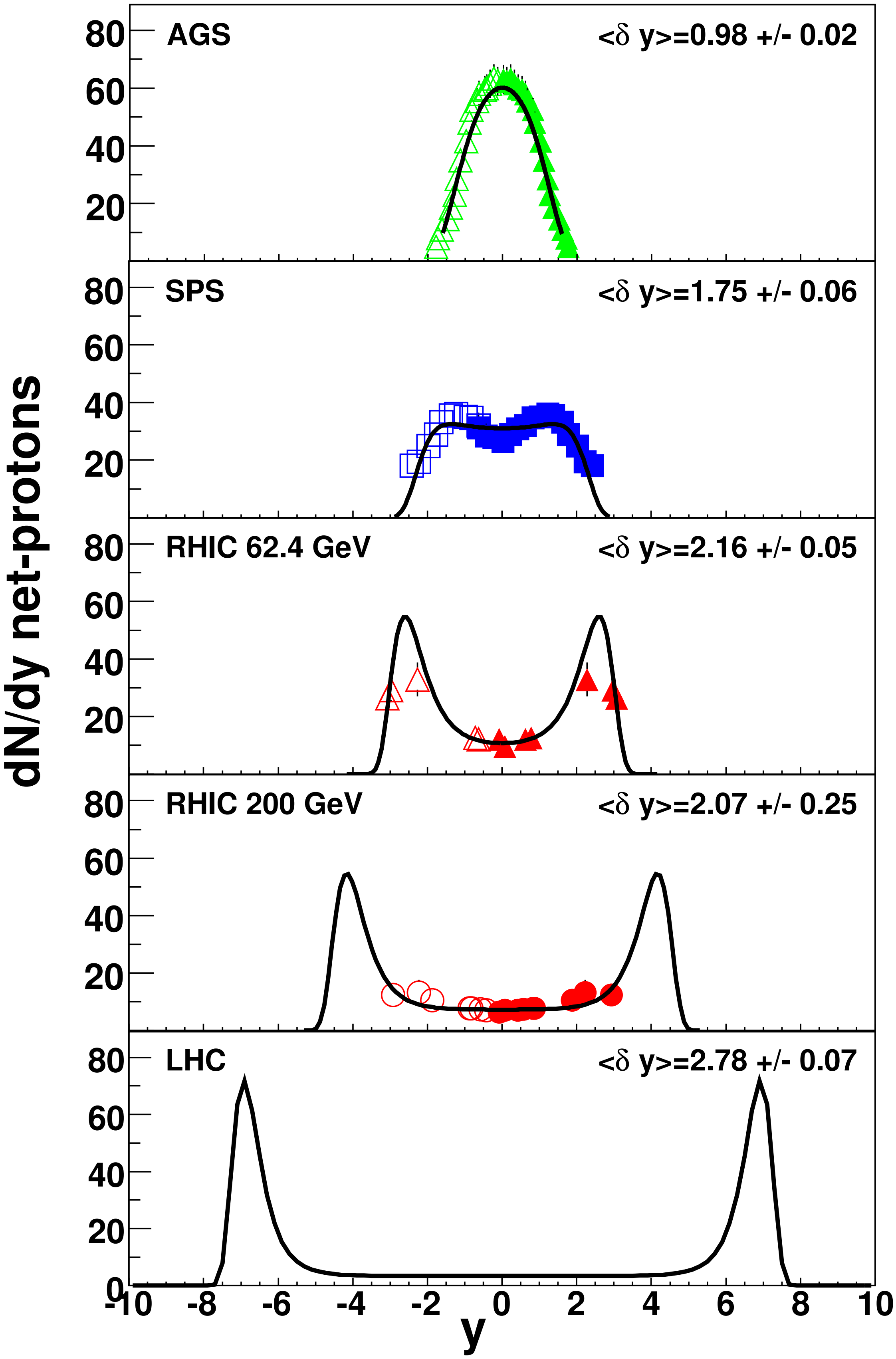

FIG. 4: The top four panels show the net proton rapidity distributions from AGS, SPS and RHIC ($\sqrt{s_{NN}}$ = 62.4 GeV and $\sqrt{s_{NN}}$ = 200 GeV) obtained as described in the text. The average rapidity losses are listed. The bottom panel shows the prediction for the Large Hadron Collider (LHC)

$-5 < y < 5$ the central multiplicity at $y = 0$ is $dN/dy \approx 1300$.

In summary, the present results for the rapidity shift of baryons(protons) for Au+Au collisions at $\sqrt{s_{NN}} = 62.4$ GeV, together with similar data at lower and higher energy permit us to rather accurately determine the onset of a collision regime where the absolute rapidity loss appears to vary slowly with beam rapidity. In particular, we predict that the rapidity loss at LHC is of the order of $\delta y = 2.8$. Although the baryon rapidity shift relative to the beam rapidity decreases, the overall energy available for particle production still increases with increasing beam energy. The microscopic mechanism related to parton-parton interactions in the colliding nuclei and their nucleons underlying the stopping of heavy nuclei still needs to be understood in detail.

This work was supported by the Office of Nuclear Physics of the U.S. Department of Energy, the Danish Natural Science Research Council, the Research Council of Norway, the Polish State Committee for Scientific Research (KBN) and the Romanian Ministry of Research.

[1] Arsene, I. *et al.*, BRAHMS Collaboration, Nucl. Physics, **A757**, 1 (2005).
[2] Adams, J. *et al.*, STAR Collaboration, Nucl. Physics, **A757**, 102 (2005).
[3] Adcox, K. *et al.*, PHENIX Collaboration, Nucl. Physics, **A757**, 184 (2005).
[4] Back, B. B. *et al.*, PHOBOS Collaboration, Nucl. Physics, **A757**, 28 (2005).
[5] Gyulassy, M. and McLerran, L., Nucl. Physics, **A750**, 30 (2005).
[6] Bearden, I. G. *et al.*, BRAHMS Collaboration, Phys. Rev. Lett., **88**, 202301 (2002).
[7] Back, B. B. *et al.*, E917 Collaboration, Phys. Rev. Lett., **86**, 1970 (2001).
[8] H. Appelhauser *et al.*, NA49 Collaboration, Phys. Rev. Lett. **82**, 2471 (1999).
[9] Bearden, I. G. *et al.*, BRAHMS Collaboration, Phys. Rev. Lett., **93**, 102301 (2004).
[10] Videbaek, F. and Hansen, O., Phys. Rev., **C52**, 1995, 2684.
[11] M. Adamczyk *et al.*, BRAHMS Collaboration, Nucl. Instr. and Meth., A499 (2003) 437.
[12] Anticic, T. *et al.*, NA 49 Collaboration, Phys. Rev. Lett., **93**, 022302 (2004).
[13] G.E. Cooper, NA 49 Collaboration, Nucl. Phys., **A661** 362, 1999.
[14] E802 Collaboration, L. Ahle *et al.*, Phys. Rev. **60**, 064901 (1999)
[15] E877 Collaboration, J. Barette *et al.*, Phys. Rev. **62**, 024901 (2000)
[16] GEANT 3.2.1, CERN program library.
[17] X. N. Wang and M. Gyulassy, Phys. Rev. D **44**, 3501 (1991).

DRAFT